On the Thrust Surface of Unreiforced and FRP-/FRCM-Reinforced Masonry Domes

Francesco Fabbrocino[1], Ilenia Farina[1], Valentino Paolo Berardi[2], A. J. M. Ferreira[3], and Fernando Fraternali[2]*,

[1]Department of Engineering, Pegaso University, Piazza Trieste e Trento, 48- 80132- Naples, Italy

[2]Department of Civil Engineering, University of Salerno, Via Giovanni Paolo II, 132, 84084 Fisciano (SA), Italy

[3]Faculdade de Engenhardia da Universidade do Porto, Porto, Portugal

August 1, 2015

Abstract

We employ a r-adaptive finite element model to search for a 'safe' thrust surface of a masonry dome, which minimizes the maximum tensile stress carried by the unreinforced portion of the material. A numerical procedure based on a Breeder Genetic Algorithm is employed to drive the movement of the nodes of a membrane model within a suitable design domain, which coincides with the region comprised in between the intrados and extrados of the dome in correspondence with the unreinforced portion of the structure. The presence of externally bonded Fiber Reinforced Polymer and/or Fabric Reinforced Cementitious Mortar reinforcements is accounted for by allowing the thrust surface to move outside the physical domain of the structure in correspondence with the reinforced regions. A benchmark example shows that the proposed procedure leads to detect if a masonry dome is safe or not, according to the master 'safe' theorem of the masonry vault theory. In addition it allows to optimally design reinforcement strategies that are aimed at preventing or mitigating crack damage, and increasing the load carrying capacity of the structure.

Keywords: Masonry Domes, Thrust Surface, R-Adaption, FRP, FRCM, Evolutionary Algorithms.

1 Introduction

The so-called modern vault theory by Heyman [1] consists of a limit analysis approach to the statics of masonry arches and vaults based on the following assumptions: (i) masonry has no tensile strength, (ii) masonry has infinite compressive strength, and (iii) sliding between masonry parts does not occur (*no-tension model*). It is well suited for curved structures where the effects of bending and shear stresses on the collapse mechanisms are usually less relevant than those played by in-plane tensile stresses [2, 3]. The individual roles played finite friction between parts, infill, brick pattern and individual members, such as, e.g., the lantern, drum and buttresses, on the limit analysis of masonry vaults and domes is accurately described in [2, 3] and references therein. In the case of masonry arches, the master 'safe' theorem of Heyman leads to search for a fully-compressive line of thrust (or funicular curve) of the applied loads, which is entirely contained within the intrados and the extrados of the structure ('static' theorem of the limit analysis of masonry arches, see Chapters 1 and 2 of [1]). Several extensions of the funicular curve method to 3D problems dealing with vaults and domes have been proposed over recent years, by using either continuous or discontinuous approaches. Continuous approaches typically make use of stress-function formulations of the equilibrium problem [4, 5, 6] or maximum modulus eccentricities surfaces [7, 8], while discontinuous approaches describe the no-tension stress field through spatial force networks generated via 3D funicular constructions [9], the Thrust Network Analysis (TNA) [10, 11], or the Lumped Stress Method (LSM) [12, 13, 14, 15]. Continuous and discontinuous approaches based

*Corresponding author: f.fraternali@unisa.it

on stress-functions or the TNA are intrinsically restricted to parallel loading [4, 13, 11], while maximum modulus eccentricities surfaces call for fixed finite element models assuming fixed boundary conditions [8]. Under parallel loading, a stress function-based mesh adaption strategy based has been presented in [13], employing a convex hull predictor-corrector strategy.

A number of studies have shown that genetic/evolutionary algorithms are particularly useful in structural optimization problems [16, 17, 18, 19, 20]. In particular, such optimization strategies have led to show that funicular shapes of curved structures provide minimal compliance configurations [21]. Optimization through evolutionary algorithms was first developed in the 1960s and has since come to refer to a family of probabilistic search methods inspired by the principle of natural selection [22, 23, 24, 25]. Evolutionary optimization algorithms have been shown to be well suited for problems where the solution space is multidimensional, multimodal, discontinuous, and noisy [26]. A Breeder Genetic Algorithm (BGA), is a specific type of evolutionary optimization algorithm, that employs a both stochastic and a deterministic selection scheme, in that the fittest "individuals" (solutions) are selected from a current generation and enter the "gene pool" to be recombined and mutated as the basis to form the new generation, fitter population, and arrive at an optimal solution [27, 28, 29, 30].

The present study deals with an adaptive finite element approach to the search for a 'safe' thrust surface of a masonry dome, which is either unreinforced, or reinforced through externally bonded Fiber Reinforced Polymer (FRP) and/or Fabric Reinforced Cementitious Mortar (FRCM) systems over a portion of the boundary [5, 6, 31, 32, 33, 34, 35, 36]. We assume that the dome resists the external loads through a thrust surface contained in a given search domain, which exhibits zero or almost-zero tensile stresses over the unreinforced portion of masonry. An elastic finite element model is allowed to move within the search domain, utilizing a BGA to manipulate the coordinates of the mesh nodes within the prescribed bounds, and minimizing the maximum tensile stress suffered by the unreinforced masonry (fitness function). The proposed approach is able to handle arbitrary loading conditions, structural inhomogeneities (e.g., nonuniform material properties), and geometries. The modeling of FRP/FRCM reinforcements is carried out following Baratta and Corbi [5, 6], on allowing the thrust surface to move outside the physical domain of the structure in correspondence with the reinforced regions. A benchmark example allows us to emphasize the technical potential of the proposed approach, which leads to design optimal placements of FRP/FRCM reinforcements, and the associated benefits in terms of crack damage prevention and load carrying capacity of the structure.

2 R-Adaptive Thrust Surface

Without loss of generality, let us refer our analysis to the dome of the church of Santa Maria di Monteverginella in Naples, which is illustrated in Figs. 1- 2. Such a dome has a variable thickness, rests on a circular drum and is crowned with a small lantern (without openings). The wall thickness varies from 0,57 m in correspondence with the drum, to more than 1,00 m at the crown (including the base of the lantern). The intrados of the dome is not decorated with frescos (nude masonry), while the extrados is covered with majolica tiles (Fig. 2). We model the dome and the top portion of the drum (below the openings) through a r-adaptive Sap2000® finite element model (FEM) with linearly elastic response. The latter is composed of 154 nodes and 272 shell elements, as shown in Fig. 3. The shell elements feature dominant membrane behavior, since their bending thickness is set equal to 1/50 of the membrane thickness [37]. We assign the masonry self-weight equal to 15.0 kN/m^3, and the Young modulus of the material equal to 1500 MPa ('Neapolitan' tufe stone masonry [38]). The basis of the dome is supposed to be restrained by fixed hinge supports. The FEM nodes are allowed to move in 3D according to the following r-adaption strategy

$$r_i \;=\; r_i^{min} \;+\; \xi_i \left(r_i^{max} \;-\; r_i^{min}\right) \tag{1}$$

where r_i denotes the radial distance of the i-th node from the associated control point C_i lying on the dome axis; r_i^{min} is the value of r_i at the intrados of the dome; r_i^{max} is the value of r_i at the extrados; and ξ is a control variable ranging in the interval $[0, 1]$ (Fig. 1).

2.1 Breeder Genetic Algorithm

To minimize the maximum tensile stress carried by the thrust surface in correspondence with unreinforced masonry we employ the BGA fully described in [29, 30, 21]. Let N denote the total number of control variables ξ_i governing the r-adaption strategy described by Eqn. (1). We create a population (generation) of $\lambda = 100$ "individuals" (solutions) $\mathbf{r}_m^t = (r_1, ..., r_N)_m$ where m is index of the individual ($m \in \{1, \cdots, \lambda\}$), and let the BGA create $G = 200$ generations where $t \in \{1, \cdots, G\}$ is the generation. The minimization of the maximum tensile stress carried by the unreinforced masonry leads the adopted FEM to approximate the elastic no-tension constitutive model (refer, e.g., to [2, 4, 7, 15] and references therein).

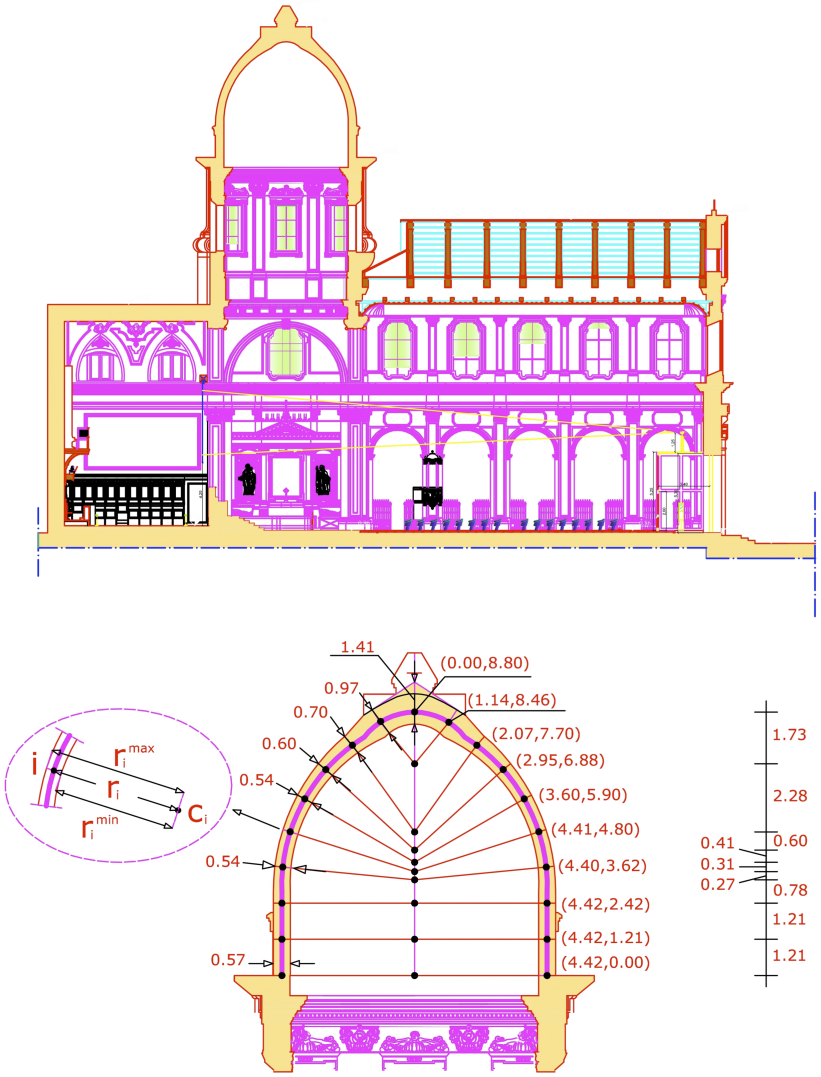

Figure 1: Cross-section of the church of Santa Maria di Monteverginella in Naples (top) and zoom-in of the dome (bottom).

Figure 2: Photographs of the exterior (left) and the interior (right) of the dome of the church of Santa Maria di Monteverginella in Naples.

2.1.1 Selection

The selection consists of the picking, at each generation, the μ best individuals within the current population of λ elements. When applying BGA, the best individual found will always be retained. The remaining $\lambda - 1$ individuals of the next generation are generated by recombining and mutating the μ best individuals of the current generation. By doing so, the best individuals are treated as super-individuals and mated together, hoping that this will lead to a fitter population. The probability of selection for recombination is

$$p = \begin{cases} \frac{1}{\mu} & 1 \leq i \leq \mu \\ 0 & \mu \leq i \leq \lambda \end{cases} \tag{2}$$

2.1.2 Recombination

To create the new generation from the μ best individuals within the current population of λ elements, we utilize Extended Intermediate Recombination (EIR) [39]. In order to define the operators, let us suppose to have two parents (each one of the μ individuals) $\mathbf{x} = (x_1, ..., x_N)$ and $\mathbf{y} = (y_1, ..., y_N)$ and one child before mutation $\mathbf{z} = (z_1, ..., z_N)$, where x_i, y_i, and z_i are the radial distances of the current note from the corresponding control node C_i (Fig. 1). Using EIR we have

$$z_i^{t+1} = x_i^t + c_i \cdot \left(y_i^t - x_i^t\right), \forall i \in \{1, ..., N\} \tag{3}$$

where c_i is a scaling factor chosen uniformly at random over an interval $[-d, 1 + d]$ where $d = 0.25$. This allows to reach all the values belonging to the continuous interval between x_i and y_i, and to exit too, for a quantity given by d. As a consequence, EIR is capable of producing any point within a hypercube slightly larger than the one defined by the parents.

2.1.3 Mutation

Offspring variables are then mutated by the addition of small random values with low probability. The probability of mutating a variable is set to be inversely proportional to the number of parameters to optimize. The mutation operator acts by modifying randomly each vector $\mathbf{z}^t$ by adding a random vector $\mathbf{q} = (q_1, ..., q_k)$, q_i being scaled according to the search interval of z_i

$$\mathbf{w}^{t+1} = \mathbf{z}^t + \mathbf{q} \tag{4}$$

The entries in $\mathbf{q}$ are uniformly distributed ($U(-\sigma; \sigma)$), where σ is defined as $a \cdot (z_{i_{max}} - z_{i_{min}})$ and a is a scale factor we choose here as 0,5. It should be noted, that when a genetic operator generates a value for a parameter out of the

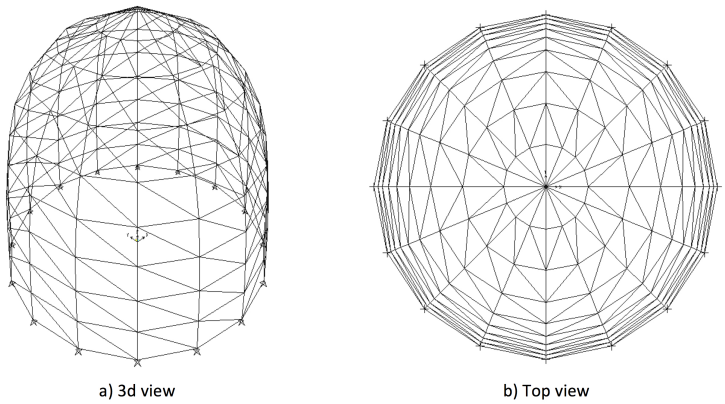

Figure 3: 3D and top views of the r-adaptive finite element model.

range, the value is reported within the range by mirroring, i.e., by adding/subtracting to it the value of the limit of the range closest to it, depending on whether it is smaller or greater than the lower/upper limit of the range. Following the selection, recombination, and mutation, the new generation is filled with children **w**.

3 Numerical Results

We examine the r-adaptive FEM described in Sect. 2 (Figs. 1- 3) under either the sole action of the masonry self-weight (*vertical loading*), and the combined action of masonry self-weight and horizontal forces acting along the x-axis of a Cartesian frame $\{O, x, y, z\}$, which shows the z axis pointing upward along the vertical direction. The analyzed horizontal forces mimic the effects of a seismic excitation along the x direction of the dome, according to a conventional, static approach to seismic actions on constructions (refer, e.g., to the European Standard EN 1998-1[40]). In particular, the horizontal forces in the x direction are set equal to 25% of vertical forces (*seismic loading*). Hereafter, we label 'RTS' the Reference Thrust Surface that passes through the nodes marked by black circles in Fig. 1, and let 'MTTS' denote the Minimum Tension Thrust Surface obtained through the BGA described in Sect. 2.1. As anticipated, the latter minimizes the maximum tensile stress in the unreinforced masonry (σ_{max}); is contained between the intrados and the extrados of the vault in correspondence to the unreinforced portion of masonry; and is allowed to move beyond the physical domain of the structure in correspondence to the FRP-/FRCM-reinforced regions, on the opposite side of the reinforcements [5, 6] (we locally assume: $r_{max} = r_{min} + 2.000$ m). It is worth noting that the the initial tensile strength of the examined masonry (undamaged material) is slightly greater than zero and ranges in the interval 0.1-1.0 MPa, while its compressive strength is approximatively equal to 13 MPa [38]. We assume that the materials and the thickness of the FRP-/FRCM-reinforcements are adequately designed, in such a way that the reinforced masonry is able to fully sustain the tensile stresses acting on the reinforced regions of masonry.

3.1 Vertical loading

Let us first examine the case of vertical loading on the unreinforced vault. Fig. 4 illustrates the geometries of the RTS and the MTTS and the associated maps of the maximum and minimum principal stresses, which we obtained for such a loading condition. The results in Fig. 4 lead us to recognize that the maximum (tensile) principal stress carried by the MTTS ($\sigma_{max} = 1.59 \times 10^{-2}$ MPa, cf. Fig. 4d) is more than 50 % smaller than that carried by the RTS ($\sigma_{max} = 3.49 \times 10^{-2}$ MPa, cf. Fig. 4c). On the contrary, the minimum (compressive) principal stress carried by the MTTS at the base of the structure ($\sigma_{min} = -3.89 \times 10^{-1}$ MPa, Fig. 4e) is more than twice larger in magnitude than

that carried by the RTS ($\sigma_{min} = -1.14 \times 10^{-1}$ MPa, Fig. 4d). It is worth noting that the largest tensile stresses act at about one half of the rise along parallel (or hoop) lines (cf. Fig. 4c-d), and that the MTTS is almost tangent to the extrados in correspondence to the base of the drum (maximum abutment thrust), and near the lantern (Fig. 4b). Such results lead us to predict a meridional crack pattern of the unreinforced vault, which is indeed frequent in masonry domes, and typically allows the structure to be safe in such a cracked state [1].

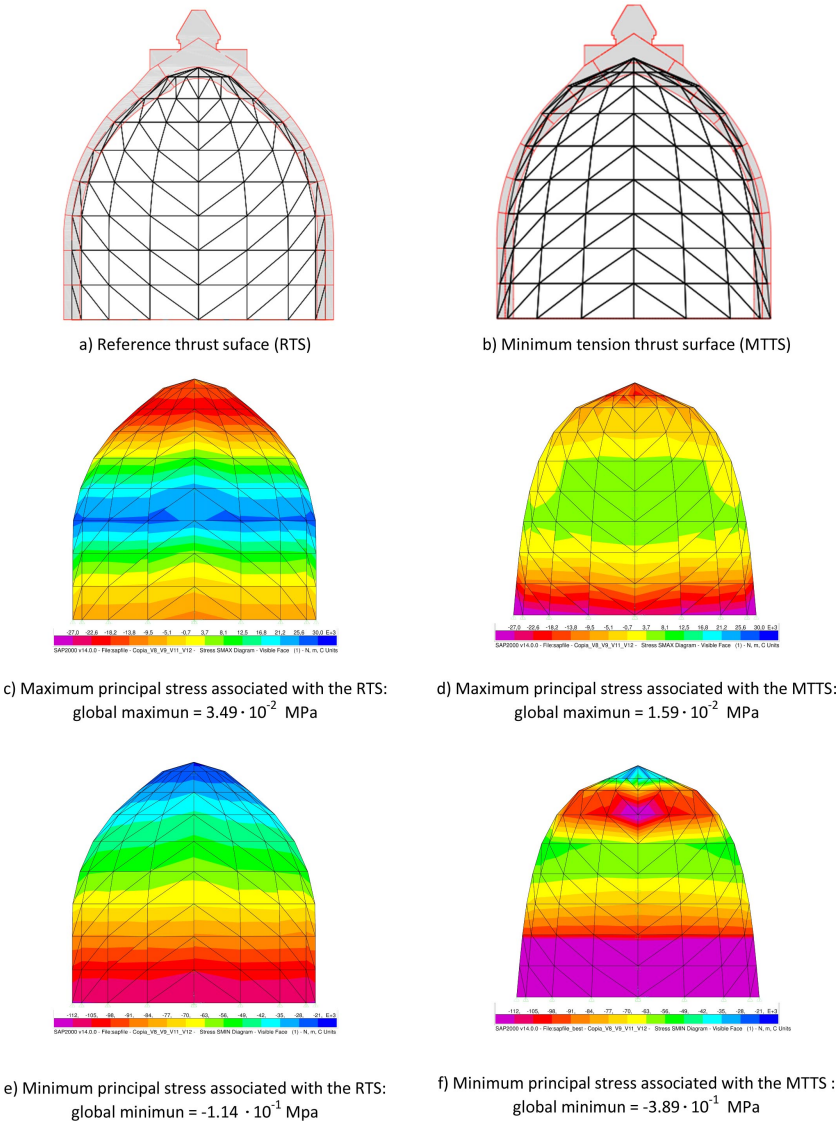

a) Reference thrust suface (RTS)

b) Minimum tension thrust surface (MTTS)

c) Maximum principal stress associated with the RTS: global maximun = $3.49 \cdot 10^{-2}$ MPa

d) Maximum principal stress associated with the MTTS: global maximun = $1.59 \cdot 10^{-2}$ MPa

e) Minimum principal stress associated with the RTS: global minimun = $-1.14 \cdot 10^{-1}$ Mpa

f) Minimum principal stress associated with the MTTS : global minimun = $-3.89 \cdot 10^{-1}$ MPa

Figure 4: Results for vertical loading of the unreinforced dome.

The results concerned with vertical loading of the FRP-/FRCM-reinforced dome are shown in Fig. 5. We examine two different reinforcement patterns: a first one featuring FRP-/FRCM-reinforcements at the top of the intrados, and a second one instead featuring FRP-/FRCM reinforcements at the interior of the drum. In both cases, the reinforcements are placed at the intrados, in correspondence to regions where the MTTS of the unreinforced dome is tangent to the extrados (Fig. 4b). As we already observed, the intrados of the examined dome is not decorated with frescos and can therefore be subjected to wrapping with FRP-/FRCM reinforcements (cf. Fig. 2).

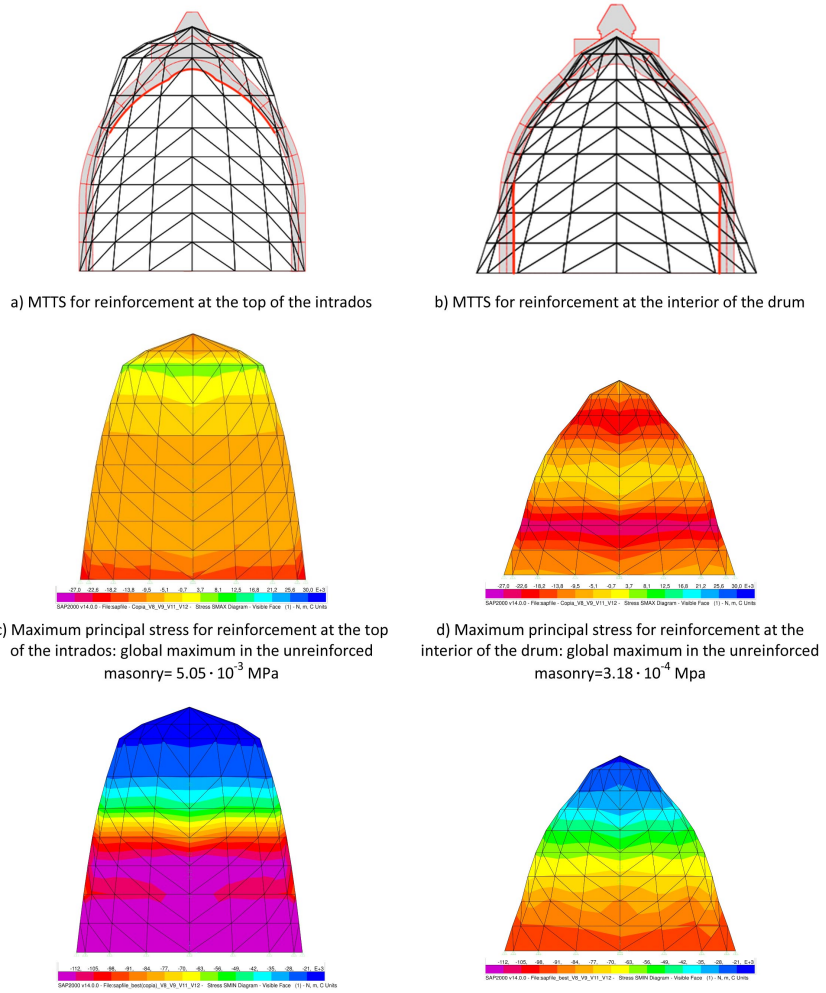

a) MTTS for reinforcement at the top of the intrados

b) MTTS for reinforcement at the interior of the drum

c) Maximum principal stress for reinforcement at the top of the intrados: global maximum in the unreinforced masonry= $5.05 \cdot 10^{-3}$ MPa

d) Maximum principal stress for reinforcement at the interior of the drum: global maximum in the unreinforced masonry=$3.18 \cdot 10^{-4}$ Mpa

e) Minimum principal stress for reinforcement at the top of the intrados: global minimjum in the unreinforced masonry= $-2.32 \cdot 10^{-1}$ MPa

f) Minimum principal stress for reinforcement at the interior of the drum: global minimjum in the unreinforced masonry=$-1.02 \cdot 10^{-1}$ Mpa

Figure 5: Results for vertical loading of the reinforced dome (thick red lines in panels a) and b) mark the positions of FRP-/FRCM-reinforcements).

The results in Fig. 5 show that the maximum tensile stress carried by the unreinforced masonry is reduced by a factor of 3 in presence of reinforcements at the top of the intrados ($\sigma_{max} = 5.05 \times 10^{-3}$ MPa, cf. Fig. 5c), and by a factor of 50 in presence of reinforcements at the interior of the drum ($\sigma_{max} = 3.18 \times 10^{-4}$ MPa, cf. Fig. 5d), always comparing with the case of the unreinforced vault ($\sigma_{max} = 1.59 \times 10^{-2}$ MPa, cf. Fig. 4d). We also observe that reinforcements at top of the intrados leave the MTTS tangent to the extrados at the base of the drum (Fig. 5a), while reinforcements at the interior of the drum push the MTTS inward at half of the rise and upward at the crown (cf. Fig. 5b and Fig. 4b). The minimum compressive stress is more than twice larger (in magnitude) in presence of reinforcements at the top of the intrados ($\sigma_{min} = -2.32 \times 10^{-1}$ MPa, Fig. 5e), as compared to the case with reinforcements at the interior of the drum ($\sigma_{min} = -1.02 \times 10^{-1}$ MPa, Fig. 5f). It is worth noting that the reinforcements can be effective under pre-existing loads only if they are adequately pretensioned before application to the masonry substrate, through e.g.. mechanical anchoring devices [41]. Alternative and more traditional reinforcement techniques of masonry domes are offered by circumferentially pre-stressed steel belts to be applied against the drum of the structure [3].

3.2 Seismic loading

We show in Fig. 6 the MTTSs that we obtained for the case of seismic loading. Trivially, such thrust surfaces do not feature polar symmetry (as in the case of vertical loading), being only symmetric with respect to the x axis. The maps of the maximum and minimum principal stresses under seismic loading are shown in Fig. 7.

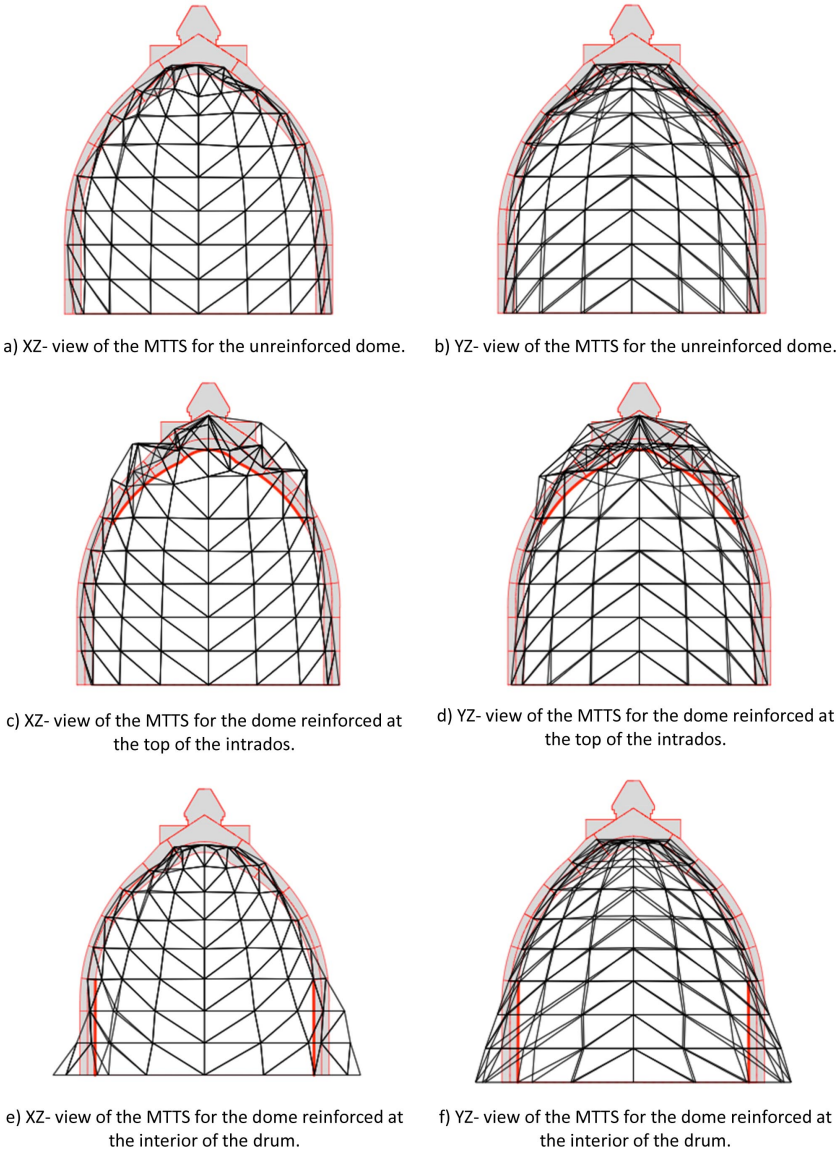

a) XZ- view of the MTTS for the unreinforced dome.

b) YZ- view of the MTTS for the unreinforced dome.

c) XZ- view of the MTTS for the dome reinforced at the top of the intrados.

d) YZ- view of the MTTS for the dome reinforced at the top of the intrados.

e) XZ- view of the MTTS for the dome reinforced at the interior of the drum.

f) YZ- view of the MTTS for the dome reinforced at the interior of the drum.

Figure 6: MTTSs for seismic loading of the unreinforced an reinforced domes.

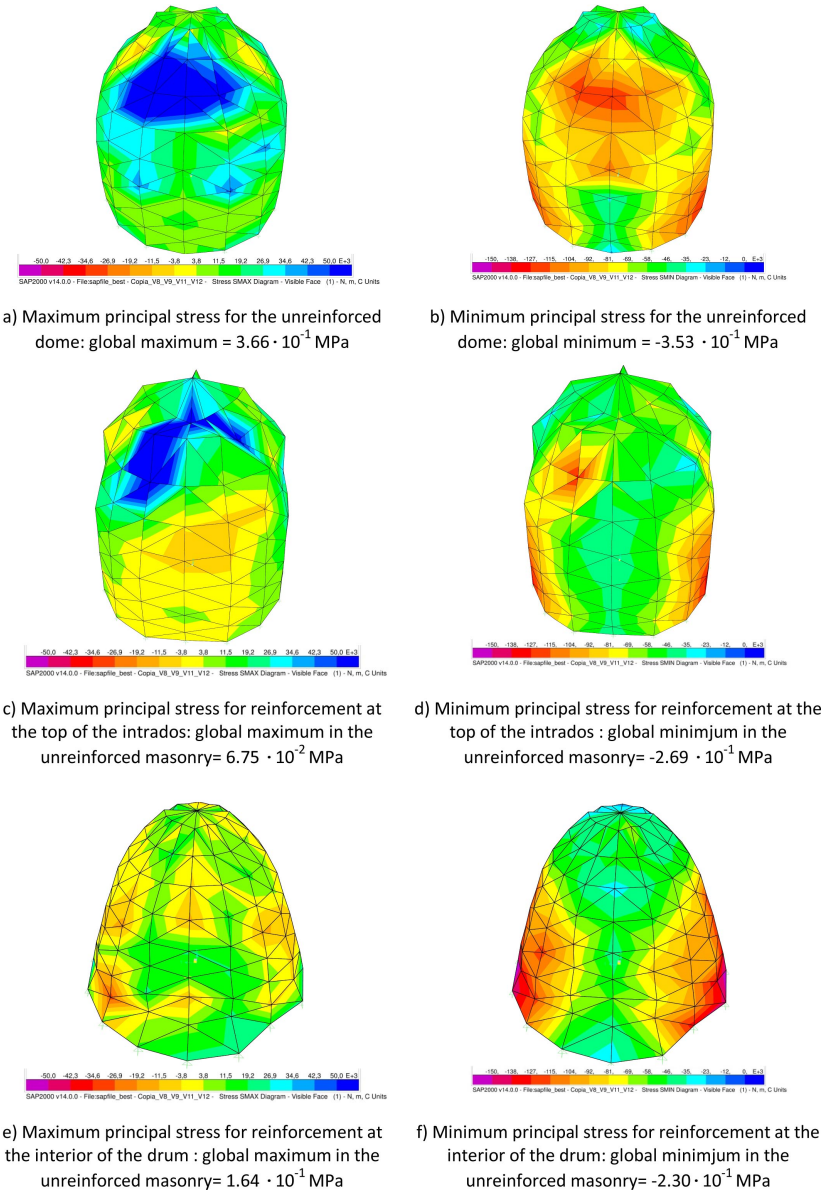

a) Maximum principal stress for the unreinforced dome: global maximum = $3.66 \cdot 10^{-1}$ MPa

b) Minimum principal stress for the unreinforced dome: global minimum = $-3.53 \cdot 10^{-1}$ MPa

c) Maximum principal stress for reinforcement at the top of the intrados: global maximum in the unreinforced masonry= $6.75 \cdot 10^{-2}$ MPa

d) Minimum principal stress for reinforcement at the top of the intrados : global minimjum in the unreinforced masonry= $-2.69 \cdot 10^{-1}$ MPa

e) Maximum principal stress for reinforcement at the interior of the drum : global maximum in the unreinforced masonry= $1.64 \cdot 10^{-1}$ MPa

f) Minimum principal stress for reinforcement at the interior of the drum: global minimjum in the unreinforced masonry= $-2.30 \cdot 10^{-1}$ MPa

Figure 7: Stress distributions for seismic loading of the unreinforced an reinforced domes.

The results in Fig. 7 highlight that the maximum tensile stress in the unreinforced masonry is reduced by a factor larger than 5 in the dome reinforced at the top of the intrados ($\sigma_{max} = 6.75 \times 10^{-2}$ MPa, cf. Fig. 7c), and by a factor slightly larger than 2 in the dome reinforced at the interior of the drum ($\sigma_{max} = 1.64 \times 10^{-1}$ MPa, cf. Fig. 7e), as compared to the case of the unreinforced dome ($\sigma_{max} = 3.66 \times 10^{-1}$ MPa, cf. Fig. 7a), under the same loading condition. We also observe marked increments of σ_{max} when passing from vertical loading to seismic loading (compare the results in Figs. 4c-d, Fig. 5c-d, and Fig. 7a,c,e). It is worth noting that the magnitude of the minimum compressive stress remains significantly lower than the compressive strength of the examined material (13 MPa, cf. [38]), both under vertical and seismic loading. Assuming that the tensile strength f_t of the unreinforced masonry is equal to $0.2 - 0.3$ MPa, we conclude that, for the unreinforced dome, it results $\sigma_{max} > f_t$, while, both for the dome reinforced at the top of the intrados and the dome reinforced at the interior of the drum, it results $\sigma_{max} < f_t$. The maximum tensile stresses act along parallel lines and reach extreme values over the edge placed in the positive

x-direction (Fig. 7a,c,e). Obviously, the opposite edge will instead suffer the maximum tensile stresses in the case of seismic loading in the negative x-direction. The reinforcement-induced reduction of the maximum tensile strength is significantly beneficial in terms of mitigation of crack damage, according to the elastic no-tension constitutive model of masonry [2, 3, 4, 7, 15].

4 Concluding Remarks

We have presented a numerical model of unreinforced and reinforced masonry domes, which searches for the optimal configuration of the thrust surface of the structure through minimization of the maximum tensile stress in the unreinforced masonry. The proposed approach employes a r-adaptive finite element model of the thrust surface featuring linearly elastic shell elements with dominant membrane behavior. The nodes of such a model are allowed to move within a given search domain, which coincides with the region physically occupied by the structure in correspondence with the unreinforced portion of the dome (no-tension model). The form-finding problem of the thrust surface is numerically approached through a Breeder Genetic Algorithm, on assuming the maximum tensile stress in the unreinforced masonry as fitness function (minimization problem).

As compared to continuous and discontinuous approaches based on stress-functions or the Thrust Network Analysis, which are intrinsically restricted to parallel loading [4, 11, 13], the present approach allows for significant technical improvements, being able to handle arbitrary loading conditions, such as, e.g., the seismic loading conditions commonly adopted by international codes for constructions [40]. It can be usefully employed to design optimal FRP- and/or FRCM-reinforcements, which are able to significantly mitigate fracture damage, and to increase the load carrying capacity of the structure.

We address generalizations of the present study dealing with masonry vaults featuring arbitrary geometries, and discrete models of membrane networks [13, 42] to future work. Additional future directions of the present research will regard the direct inclusion of FRP-/FRCM-reinforcements in the proposed form-finding strategy, withe the aim of designing optimal reinforcement topologies under prescribed constraints on structural stability, nature of the failure modes and 'pseudo-ductility' of the material [3]. Finally, in a near future we intend to conduct experimental validations of the present study through static and dynamic testing of real-scale models of vaults and domes [43, 44, 45].

Acknowledgments

The authors wish to acknowledge the great support received by Gerardo Carpentieri, Giuseppe Teodosio, Luca Crescenzo and Mariella De Piano (Department of Civil Engineering, University of Salerno, Italy) during the course of the present work.

References

[1] Heyman J. *The stone skeleton*. Cambridge University Press, New York, 1995.

[2] Tralli A., Alessandri C., Milani, G. Computational methods for masonry vaults: a review of recent results. *Open J Civ Eng 2014*; 8(1):272–287.

[3] Foraboschi, P. Resisting system and failure modes of masonry domes. *Eng Fail Anal 2014*; 44:315–337.

[4] Baratta A., Corbi, O. On the equilibrium and admissibility coupling in NTV vaults of general shape. *Int J Solids Struct 2010*; 47(17):2276–2284.

[5] Baratta A., Corbi, O. An approach to the positioning of FRP provisions in vaulted masonry structures. *Compos Part B-Eng 2013*; 53:334–341.

[6] Baratta A., Corbi, O. Closed-form solutions for frp strengthening of masonry vaults. *Comput Struct 2015*; 147, 244–249.

[7] Lucchesi M., Padovani C., Pasquinelli G., Zani N.. The maximum modulus eccentricities surface for masonry vaults and limit analysis. *Math Mech Solids 1999*; 4(1):71–87.

[8] Lucchesi M., Padovani C., Pasquinelli G., Zani N.. Static analysis of masonry vaults, constitutive model and numerical analysis. *J Mech Mater Struct 2007*; 2(2):221–244.

[9] O'Dwyer, D. Funicular analysis of masonry vaults. *Comput Struct 1999*; 73(1-5):187–197.

[10] Block P., Lachauer L., Rippmann, M. *Thrust network analysis: Design of a cut-stone masonry vault*. In *Shell Structures for Architecture: Form Finding and Optimization 2014*; 71–87.

[11] Block P., Lachauer L. Three-dimensional funicular analysis of masonry vaults. *Mech Res Commun 2014*; 56:53–60.

[12] Fraternali F., Angelillo A., Fortunato F. A lumped stress method for plane elastic problems and the discrete-continuum approximation. *Int J Solids Struct 2002*; 39:6211–6240.

[13] Fraternali F. A thrust network approach to the equilibrium problem of unreinforced masonry vaults via polyhedral stress functions. *Mech Res Commun 2010*; 37(2):198–204.

[14] Fraternali F. A mixed lumped stress-displacement approach to the elastic problem of masonry walls. *Mech Res Commun 2011*; 38(3):176–180.

[15] Angelillo M., Fortunato A., Montanino A., Lippiello, M.. Singular stress fields in masonry structures: Derand was right. *Meccanica 2014*; 49(5):1243–1262.

[16] Golberg D. E., Samtani M.P. Engineering optimization via genetic algorithm. *Proc., 9th Conf. Electronic Computation, ASCE 1986*; pages 471–482.

[17] Jenkins, W.M.. Plane frame optimum design environment based on genetic algorithm. *J Struct Eng–ASCE 1992*; 118.

[18] Hajela P., Lee E., Lin C. Y. . Genetic algorithms in structural topology optimization. In C. A. Mota Soares M. P. Bendsøe, editor, *Topology Design of Structures 1990*; volume 227, pages 117–133. Kluwer Academic Publishers, Dordrecht. NATO ASI Series E: Applied Sciences.

[19] Chapman C. D. , Saitou K., Jakiela M. J. Genetic algorithms as an approach to configuration and topology design. *J Mech Design 1994*; 116:1005–1012.

[20] Rajan S. D.. Sizing, shape and topology design optimization of trusses using genetic algorithm. *J Struct Eng–ASCE 1995*; 121(10):1480–1487.

[21] Fraternali F., Porter M.A., Daraio, C. *Mech Adv Mat Struct 2010*;1(1).

[22] Holland, J.H.. Outline for a logical theory of adaptive systems. *J ACM 1962*, 9(3):297–314.

[23] Fogel L.J., Owens A. J., Walsh M. J. *Artificial Intelligence through Simulated Evolution 1966*; John Wiley, New York.

[24] Goldberg D. E., Holland J.H. Genetic algorithms and machine learning. *Mach Learn 1988*;3:95–99.

[25] Mitchell M. Forrest S. Genetic algorithms and artificial life. *Artifl Life 1994*; 1(3):267–289.

[26] DeJong K. Evolutionary computation: a unified approach. In *GECCO 2007*; 3158–3171.

[27] Muhlenbein H., Schlierkamp-Voosen D. The science of breeding and its application to the breeder genetic algorithm (bga). *Evolu Comput 1993*; 1(4):335–360.

[28] Muhlenbein H., Schlierkamp-Voosen D. Predictive models for the breeder genetic algorithm, i: Continuous parameter optimization. *Evolu Comput 1993*; 1(1):25–49.

[29] De Falco I, Del Balio R., Della Cioppa A., Tarantino E. A comparative analysis of evolutionary algorithms for function optimisation. In *Proceedings of the Second Workshop on Evolutionary Computation (WEC2)1996*; 29–32. Nagoya, JAPAN.

[30] De Falco I, Del Balio R., Della Cioppa A., Tarantino E. Optimising constrained continuous multivariable functions with breeder genetic algorithms. In *In S. Kundu Evolutionary Optimization 1999, 53–64 , Polish Academy of Sciences Publisher*.

[31] Ascione L., Feo L., Fraternali F. Load carrying capacity of 2D FRP/strengthened masonry structures, Compos Part B-Eng 2005; 36(8): 619–626.

[32] Caporale A., Feo L., Luciano R., Penna R. Numerical collapse load of multi-span masonry arch structures with FRP reinforcement, Compos Part B-Eng 2013; 54(1): 71–84.

[33] Foraboschi P., Vanin A.. New methods for bonding FRP strips onto masonry structures: experimental results and analytical evaluations. *Composites*, 4(1), 2013.

[34] D'Ambrisi A., Mezzi M., Feo L., Berardi V.P. Analysis of masonry structures strengthened with polymeric net reinforced cementitious matrix materials, Compos Struct 2014; 113(1): 264–271.

[35] Ascione F. Ultimate behaviour of adhesively bonded FRP lap joints Compos Part B-Eng 2013; 40(2): 107–115.

[36] Ascione, F. Mechanical behaviour of FRP adhesive joints: A theoretical model Compos Part B-Eng 2013; 40(2): 116–124.

[37] CSI. *Analysis Reference Manual for SAP2000®*. Computers and Structures 2013; Inc., Berkeley, California, USA.

[38] Manfredi G., Marcari G., Voto S. Analisi e caratterizzazione meccanica di murature di tufo. In *Proocedings of the 15th C.T.E. Congress 2004*; Bari, Nov. 4-6.

[39] Mühlenbein H., Schomisch M., Born, J.. The parallel genetic algorithm as function optimizer. *Parallel Comput 1991*; 17(6-7):619–632.

[40] European Committee for Standardization. *Eurocode 8: Design of structures for earthquake resistance ï£¡ Part 1: General rules, seismic actions and rules for buildings 2004*. EN 1998-1:2004, Brussels, Belgium.

[41] Italian National Research Council (CNR). *Guide for the Design and Construction of Externally Bonded FRP Systems for Strengthening Existing Structures - Materials, RC and PC structures, masonry structures 2013*. CNR-DT 200/2013 - R1, Rome, Italy.

[42] Schmidt B., Fraternali F. Universal formulae for the limiting elastic energy of membrane networks, *J. Mech Phys Solids 2012*; 60, 172–180.

[43] Cakir F., Seker B.S., Durmus A., Dogangun A., Uysal H. Seismic assessment of a historical masonry mosque by experimental tests and finite element analyses, *KSCE Journal of Civil Engineering*, Online first, doi=10.1007/s12205-014-0468-4.

[44] Giamundo V., Lignola G.P., Maddaloni G., Balsamo A., Prota, A. Manfredi, G. Experimental investigation of the seismic performances of IMG reinforcement on curved masonry elements, Compos Part B-Eng 2014; 70, 53–63.

[45] Modano M., Fabbrocino F., Gesualdo A., Matrone G., Farina I., Fraternali F. On the forced vibration test by vibrodyne. *CompDyn 2015*, 25-27 May 2015.